

# Coupling loss at the end connections of REBCO stacks: 2D modelling and measurement

Shuo Li<sup>1,2</sup>, Enric Pardo<sup>2\*</sup>, Ján Kováč<sup>2</sup>

<sup>1</sup> College of Information Science and Engineering,  
Northeastern University, 110004 Shenyang, China.

<sup>2</sup> Institute of Electrical Engineering, Slovak academy of sciences,  
84104 Bratislava, Slovakia.

January 10, 2020

## Abstract

In high power density superconducting motors, superconducting tapes are usually stacked and connected together at terminals to improve the current capacity. When a parallel sinusoidal magnetic field is applied on this partially coupled stack, the coupling current is induced and causes additional coupling loss. Usually 3D modeling is needed to calculate the coupling loss but it takes too much computing resource and time. In this paper, a numerical 2D modeling by minimum electromagnetic entropy production (MEMEP) method is developed to speed up the calculation. The presented MEMEP model shows good accuracy and the capability to take the realistic resistance between tapes into account for coupling loss calculation with a high number of mesh element, which agrees to measurements. Thanks to the model, a systemic study of coupling loss on amplitude-dependence, frequency-dependence, resistance-dependence, and length-dependence, is presented and discussed. The results reveal the features of coupling loss which is very helpful devices with multi-tape conductors, such as the stator or rotor windings of motors.

*Keywords:* Magnetization loss, Coupling loss, Partially coupled stack, frequency dependence, resistance dependence.

## 1 Introduction

Since the discovery of high temperature superconductivity over 30 years ago, there has been great interest in utilizing high temperature superconducting materials to develop high power density motor for aircraft to reduce the pollutant

---

\*Author to whom correspondence should be sent. Email: enric.pardo@savba.sk

emission of airplanes [1–3]. In the stator of superconducting motors, using closely packed parallel tapes as conductor improves the current capacity while keeping high engineering current densities [3]. Isolating the tapes along their length reduces the AC loss compared to non-insulated tapes, also when the tapes are connected at the current terminals [3,4]. This we name this kind of stack is as partially coupled stack.

A sketch of the partially coupled stack is shown in Figure 1(b). When a parallel time-varying magnetic field is applied to the partially coupled stack, coupling current is induced and additional coupling loss is generated because of these connections. Often, the coupling loss is thousands times higher than superconducting loss. To predict the coupling loss, usually a 3D model is necessary to solve this problem [5,6]. Right now, commercial finite-element methods (FEM) with H-formulation and T-A formulation are very popular and flexible in superconducting modeling [7–11]. However, it takes too much computing resource and time, which is not suitable to model the coupling loss of the partially coupled stack with realistic resistance at terminals.

In this study, a numerical 2D model by Minimum Electro-Magnetic Entropy Production method (MEMEP) with consideration of realistic resistance between tapes is developed to solve the 3D problem. The presented MEMEP model shows good accuracy and capability, which is verified by measurements. The MEMEP method is much faster than the H-formulation and T-A formulation methods, so that it can adopt much better mesh strategy to get high precision results [12–17]. Although MEMEP has been applied to full 3D problems, it requires either high computing resources (several computers working in parallel by MPI) [15, 18]) or high computing time. Therefore, fast and accurate 2D modeling enables analyzing complex structures, such as stacks of many tapes or coils made of these stacks.

Besides, when the resistance between tapes is extremely large, the tapes are fully insulated from each other, which is called uncoupled stack, as seen in Figure 1(a). Conversely, when the resistance is extremely small, the tapes are connected very well from each other, which is called fully coupled stack, as seen in Figure 1(c). Although, uncoupled stacks (and coils) and fully coupled stacks have been well studied by many researchers before, the case of an intermediate finite resistance (“partial coupling”) has not been previously studied for stacks of tapes. Previous studies focused on ac loss under perpendicular magnetic field [19–27], ac loss under transport current [28–32], ac loss with consideration of ferromagnetic material [33–36], dynamic resistance under various applied field [37–40], magnetization and decay of trapped magnetic field [41–48], multifilamentary calculations [19, 49], among other topics.

Thanks to the presented numerical 2D MEMEP model, this article systematically studies and discusses the amplitude-dependence, frequency-dependence, and resistance-dependence of coupling loss under parallel magnetic field. The results reveal the features of coupling loss, which will be very helpful in future design considerations of power applications, such as superconducting motors, and magnets. However, rather than the particular modeling results, the main innovation of this article is the fast and accurate 2D modeling method and

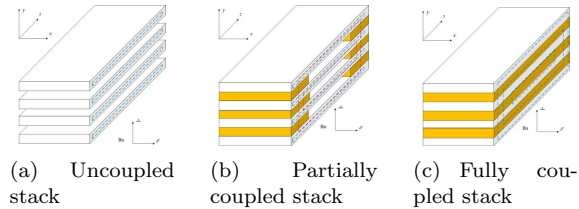


Figure 1: The sketch of proposed three kinds of superconducting stack. (a) Uncoupled stack, inducing current flows in tapes independently. (b) Partially coupled stack, inducing current flows in tapes parallel but coupled at terminals. (c) Fully coupled stack, inducing current flows in the entire cross section.

developed software to take coupling currents into account, avoiding complex time-consuming 3D modeling.

The structure of this paper is the following. The details of superconducting samples are described and measurement setup is presented in section 2. Then, the general rule of 2D minimum electromagnetic entropy production method and coupling loss modeling for the partially stack with realistic resistance at terminals are presented in Section 3 and Section 4, respectively. Magnetization loss of uncoupled and partially coupled stack samples are measured under applied sinusoidal magnetic field with a series of amplitude and frequency to verify the presented numerical 2D MEMEP model. Then, the amplitude-dependence, frequency-dependence, and resistance-dependence of coupling loss of partially coupled stack under parallel magnetic field are systematically discussed in Section 5. At last, some conclusions are given in Section 6. In the appendix, an analytical modeling of coupling loss for partially stack with four tapes at low frequency and with two tapes for any frequency are deduced in A and B, respectively.

## 2 Samples and measurement setup

### 2.1 Samples

For this work, REBCO superconducting stacks are systematically investigated (REBCO stands for  $REBa_3Cu_3O_{7+x}$ , where  $RE$  is a rare earth element, usually yttrium or gadolinium). The nonmagnetic superconducting tapes are provided by SuperOx, whose critical current is about 160 A at 77 K under self-field, and the cross section is 4 mm width times 0.2 mm thick.

Two 100 mm long superconducting stack samples are fabricated. One sample is an uncoupled stack, where four superconducting tapes are vertically “Face to Back” stacked together with 1.5 mm thick G10 to keep the gap between tapes. Another sample is a partially coupled stack with the same configuration as uncoupled stack, but the superconducting tapes are soldered together with conventional conductor at terminals with measured average resistance  $R_{av} =$



Figure 2: A photograph of the superconducting stack samples.

Table 1: The specific parameters of superconducting tape and stacks

Parameters	Value
Critical current [A]	160
$n$ -value	30
Width of tape [mm]	4
Thickness of tape [mm]	0.2
Thickness of superconductor layer [ $\mu\text{m}$ ]	2
Number of tapes in stack	4
Gap of tapes [mm]	1.5
Length of stacks [mm]	100
Average resistance at ends [ $\mu\Omega$ ]	3.13

$3.13 \times 10^{-6} \Omega$ . The soldering parts length is about 5 mm on each side of terminals. The detail parameters of superconducting tape and stacks are given in Table 1 and a photograph of stack samples is shown in Figure 2

## 2.2 Measurement setup

A photograph of the measurement system is shown in Figure 3. A DSP lock-in amplifier 7265 (EG&G Instruments) is used as a basic measuring device. Then, the signal from its internal generator is utilized as the input signal for power audio amplifier QSC RMX 1450. Copper-wound electro-magnets are then powered through a toroidal power transformer with ferromagnetic core. The

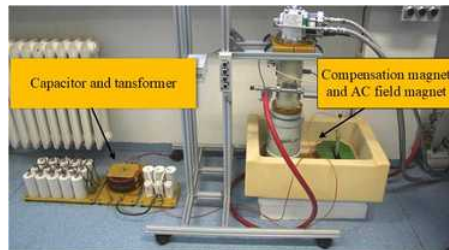


Figure 3: A photograph of the measurement system

whole coil system is immersed in liquid nitrogen to keep this magnetic system operating at 77 K. In this way, the change of impedance of the secondary due to its heating is excluded. A sinusoidal external field in the range of 1 ~ 100 mT and frequency in the range of 2 ~ 576 Hz is applied by the background electro-magnet. The magnetic field homogeneity in the sample space is less than 1%. The magnetization loss could be measured directly when the sample is placed in the center of the coil. More detail about this measurement system can be found in previously work [50].

### 3 Minimum Electro-Magnetic Entropy Production method

Generally, for any non-linear  $\mathbf{E}(\mathbf{J})$  relation of the material and Coulomb's gauge ( $\nabla \cdot \mathbf{A} = 0$ ) for the vector potential, the current density follows,

$$\mathbf{E}(\mathbf{J}) = -\frac{\partial \mathbf{A}_J}{\partial t} - \frac{\partial \mathbf{A}_a}{\partial t} - \nabla \phi. \quad (1)$$

where  $\mathbf{A}_J$  is the vector potential created by the current density  $\mathbf{J}$ . This quantity is [51]

$$\mathbf{A}_J(\mathbf{r}) = \frac{\mu_0}{4\pi} \int_{\Omega_{3D}} \frac{\mathbf{J}(\mathbf{r}')}{|\mathbf{r} - \mathbf{r}'|} d^3\mathbf{r}' \quad (2)$$

for three-dimensional (3D) modeling, where  $\mu_0$  is the vacuum permeability<sup>1</sup>,  $\mathbf{r}$  and  $\mathbf{r}'$  are the position of the observation point and generating point, respectively, and  $\Omega_{3D}$  is the region where there are currents of the 3D object of study.

The second item in Table 1,  $\mathbf{A}_a$ , is the ‘‘applied vector potential’’ or vector potential created by any applied magnetic field,  $\mathbf{B}_a$ , due to sources (currents or magnetic poles) that are external to the sample domain  $\Omega_{3D}$  and independent on the currents in  $\Omega_{3D}$ . In general,  $\mathbf{B}_a$  does not need to be uniform. In case of uniform  $\mathbf{B}_a$ , with components only in the  $x$  and  $y$  directions, the applied vector potential can be written as

$$\mathbf{A}_a = (B_{a,x}y - B_{a,y}x)\mathbf{e}_z, \quad (3)$$

which follows Coulomb's gauge. Although there are other possible ways to express this vector potential, such as  $\mathbf{A}_a = \mathbf{B}_a \times \mathbf{r}$ , we choose the option above for convenience later one.

Solving the equation above is the same as minimizing the following functional for the change of current density between two time steps [15]. After time

---

<sup>1</sup>In this article, we take a value of the vacuum permeability of  $\mu_0 = 4\pi \cdot 10^{-7}$  H/m. Strictly speaking, this is not an exact value because, according to the 2019 definition of SI,  $\mu_0$  is a measured constant.

discretization, this functional is

$$F = \int_{\Omega_{3D}} \left[ \frac{1}{2} \frac{\Delta \mathbf{A}_J}{\Delta t} \cdot \Delta \mathbf{J} + \frac{\Delta \mathbf{A}_a}{\Delta t} \cdot \Delta \mathbf{J} + U(\mathbf{J}_0 + \Delta \mathbf{J}) + \nabla \varphi \cdot (\mathbf{J}_0 + \Delta \mathbf{J}) \right] d^3 \mathbf{r} \quad (4)$$

where,  $\mathbf{J}_0$  and  $\mathbf{J}$  are the current density at times  $t = t_0$  and  $t = t_0 + \Delta t$ , respectively (This  $\Delta t$  does not need to be uniform),  $\Delta \mathbf{J} = \mathbf{J} - \mathbf{J}_0$  is the change of current density between two time steps,  $\Delta \mathbf{A}_J / \Delta t$  is the average time derivative between  $t = t_0$  and  $t = t_0 + \Delta t$  of the vector potential generated by the current density in the sample,  $\Delta \mathbf{A}_a / \Delta t$  is the same quantity but relative to the applied vector potential, and  $\varphi$  is the electrostatic scalar potential.

The dissipation factor in (4),  $U(\mathbf{J})$ , is defined as,

$$U(\mathbf{J}) \equiv \int_0^{\mathbf{J}} d\mathbf{J}' \cdot \mathbf{E}(\mathbf{J}') \quad (5)$$

which is uniquely defined because  $\nabla_{\mathbf{J}} \times \mathbf{E}(\mathbf{J}) = 0$  for any physical  $\mathbf{E}(\mathbf{J})$ , and hence  $U$  follows the property that  $\nabla_{\mathbf{J}} U(\mathbf{J}) = \mathbf{E}(\mathbf{J})$  [12]. For a small  $\Delta \mathbf{J}$ , the dissipation factor is a measure of the energy dissipation due to  $\Delta \mathbf{J}$ , since  $U(\mathbf{J}_0 + \Delta \mathbf{J}) - U(\mathbf{J}_0) \approx \Delta \mathbf{J} \cdot \mathbf{E}(\mathbf{J}_0)$ . With this definition of the dissipation factor, it can be seen that the functional of Table 7 always presents a minimum and it is unique [15].

Usually, superconductors can be approximated by a Power Law  $\mathbf{E}(\mathbf{J})$  relation and the conventional conductor could be approximated by a linear  $\mathbf{E}(\mathbf{J})$  relation; and hence

$$\mathbf{E}(\mathbf{J}) = \begin{cases} \frac{E_c}{J_c} \left| \frac{J}{J_c} \right|^{n-1} \mathbf{J}, & \text{for the superconductor} \\ \rho \cdot \mathbf{J}, & \text{for the conventional conductor} \end{cases} \quad (6)$$

Above,  $E_c$  defines the critical current criterion, since  $|\mathbf{E}| = E_c$  when  $|\mathbf{J}| = J_c$ , being  $E_c$  usually set as  $E_c = 10^{-4}$  V/m;  $J_c$  is critical current density of superconductors; and  $\rho$  is a constant conductivity. Thus, the dissipation factor of Table 6 becomes,

$$U(\mathbf{J}) = \begin{cases} E_c \frac{J_c}{n+1} \left| \frac{J}{J_c} \right|^{n+1} & \text{for the superconductor} \\ \frac{1}{2} \rho \mathbf{J}^2 & \text{for the conventional conductor.} \end{cases} \quad (7)$$

For shapes infinitely long in the  $z$  direction, the current density follows  $\mathbf{J}(\mathbf{r}) = J(x, y) \mathbf{e}_z$ , and hence  $\mathbf{A}(\mathbf{r})_J = A_J(x, y) \mathbf{e}_z$  and  $\mathbf{E}(\mathbf{r}) = E(x, y) \mathbf{e}_z$ . From this,  $\mathbf{A}_a$  of Table 3, and Table 1 we also see that  $\nabla \varphi(\mathbf{r}) = \partial_z \varphi \mathbf{e}_z$  with uniform  $\partial_z \varphi$  for each conductor (for multiple conductors). If the conductors are all of the same length  $l$ ,  $\partial_z \varphi$  is related to the voltage drop along the whole length,  $V$ ,

as  $V = -l\partial_z\varphi$ , where we define the positive current sign as that following the positive  $z$  direction. Then, the functional of Table 4 becomes

$$F = l \int_{\Omega_{2D}} \left[ \frac{1}{2} \frac{\Delta A_J}{\Delta t} \Delta J + \frac{\Delta A_a}{\Delta t} \Delta J + U(J_0 + \Delta J) \right] d^2\mathbf{r} - \sum_i^{n_t} V_i I_i. \quad (8)$$

Above,  $\Omega_{2D}$  is the domain comprising the cross-section of all conductors  $n_t$  is the number of conductors (or tapes, in our case);  $i$  labels each conductor; and  $V_i$  and  $I_i$  are the voltage drop and net current for each conductor, respectively, at time  $t_0 + \Delta t$ , being the time that we solve the current density. In Table 8,  $A_J$  in Coulomb's gauge can be written as [51]

$$A_J(\mathbf{r}) = -\frac{\mu_0}{2\pi} \int_{\Omega_{2D}} d^2\mathbf{r}' J(\mathbf{r}') \ln|\mathbf{r} - \mathbf{r}'|. \quad (9)$$

If the current constrains,  $I_i$ , are given and the minimization method respects the current constrain, the last term of Table 8 could be dropped from the functional [12]. However, for the partially coupled case, these constrains are not fixed, and hence we needed to develop the method explained in the next section.

## 4 Coupling loss modeling

The magnetization loss of the two coupling limits of uncoupled stack and fully coupled stack can be computed by minimizing the functional of Table 8 directly with some additional conditions to distinguish these two stacks [12]. However, we need to take further considerations when the tapes are joined by a finite resistance (partial coupling), as follows.

For partially coupled stack, superconducting tapes are connected together at terminals and the coupling current is induced when a parallel time-varying magnetic field is applied. The induced current appears not only in the superconductors but also in the resistance between tapes. The coupling current causes coupling loss and modifies the net current in each superconductor. To take the coupling currents into account, we should consider the full 3D formulation of Table 4. However, we can make several important simplifications, as follows. First, we can separate the current-density into that from the superconductor,  $J_s$ , and that in the resistive material,  $J_R$ . When doing so, the functional of Table 4 can be separated into

$$F = F_S + F_R + F_{RS}, \quad (10)$$

where  $F_S$  and  $F_R$  are the functional contributed from the superconductor and resistive material, respectively, and  $F_{RS}$  represents their mutual interaction.

Since the superconducting tapes are very long, we can use the 2D infinitely long assumption for  $F_S$ , resulting in [see Table 8]

$$F = l_s \int_{\Omega_{2D,s}} \left[ \frac{1}{2} \frac{\Delta A_s}{\Delta t} \Delta J_s + \frac{\Delta A_a}{\Delta t} \Delta J_s + U(J_{s0} + \Delta J_s) \right] d^2\mathbf{r} - \sum_i^{n_t} V_i I_i. \quad (11)$$

where  $l_s$  is the length of each tape,  $\Omega_{2D,s}$  is the cross-sectional region of all superconducting material, and  $\Delta A_s$  is the vector potential created by  $\Delta J_s$ .

For the resistive material, we take the 3D functional by now, being

$$F_R = \int_{\Omega_{3D,R}} \left[ \frac{1}{2} \frac{\Delta \mathbf{A}_R}{\Delta t} \cdot \Delta \mathbf{J}_R + \frac{\Delta \mathbf{A}_a}{\Delta t} \cdot \Delta \mathbf{J}_R + U(\mathbf{J}_R) + \nabla \varphi \cdot \mathbf{J}_R \right] d^3 \mathbf{r}, \quad (12)$$

where  $\Omega_{3D,R}$  is the 3D domain where there is resistive material,  $\Delta \mathbf{A}_R$  is the vector potential generated by  $\Delta \mathbf{J}_R$ , and  $\mathbf{J}_R$  is the current density in the resistive material at time  $t_0 + \Delta t$ . Next, we assume large enough resistivity (or low enough frequency) to neglect dynamic effects. Then,

$$F_R \approx \int_{\Omega_{3D,R}} d^3 \mathbf{r} U(\mathbf{J}_R) + \int_{\Omega_{3D,R}} d^3 \mathbf{r} \nabla \varphi \cdot \mathbf{J}_R. \quad (13)$$

Next, we consider a single resistance only. From Table 6, the dissipation factor follows  $U(\mathbf{J}_R) = \rho \mathbf{J}_R^2 / 2$ , which due to Ohms law ( $\mathbf{E} = \rho \mathbf{J}$ ) it becomes  $U(\mathbf{J}_R) = \mathbf{E} \cdot \mathbf{J}_R / 2$ . Since this is the local dissipation, the volume integral of  $\mathbf{E} \cdot \mathbf{J}_R$  needs to equal to the power dissipation of the resistance, being  $RI_R^2$ . Then, the first integral in Table 13 is  $RI_R^2 / 2$  for any shape of the resistive connection. The second term in Table 13 can also be simplified. Using  $\nabla \cdot (\varphi \mathbf{J}_R) = \nabla \varphi \cdot \mathbf{J}_R + (\nabla \cdot \mathbf{J}_R) \varphi$  and  $\nabla \cdot \mathbf{J}_R = 0$ , the second integral of Table 13 becomes

$$\int_{\partial \Omega_{3D,R,1}} \varphi \mathbf{J}_R \cdot d\mathbf{s} = (\varphi_o - \varphi_i) I_R = -V_R I_R, \quad (14)$$

where  $\Omega_{3D,R,1}$  is the region where a single resistance exists. At the first equality of Table 14 we used that the input and output surfaces of the current are equipotentials and at the second equality we used the standard definition of the voltage drop in the resistance,  $V_R$ . Therefore, under the static assumption Table 12 for a single resistance becomes

$$F_R \approx \frac{1}{2} RI_R^2 - V_R I_R \quad (15)$$

for any 3D shape of the resistive material with overall resistance  $R$ . If there are  $n_R$  resistances, the total functional for the resistances is

$$F_R \approx \sum_j^{n_R} \left[ \frac{1}{2} R_j I_j^2 - V_j I_j \right]. \quad (16)$$

The interaction term,  $F_{RS}$ , is

$$\begin{aligned} F_{RS} &= \int_{\Omega_{3D}} d^3 \mathbf{r} \left[ \frac{1}{2} \Delta \mathbf{J}_s \cdot \frac{\Delta \mathbf{A}_R}{\Delta t} + \frac{1}{2} \Delta \mathbf{J}_R \cdot \frac{\Delta \mathbf{A}_s}{\Delta t} \right] \\ &= \int_{\Omega_{3D}} d^3 \mathbf{r} \Delta \mathbf{J}_s \cdot \frac{\Delta \mathbf{A}_R}{\Delta t} \approx 0. \end{aligned} \quad (17)$$



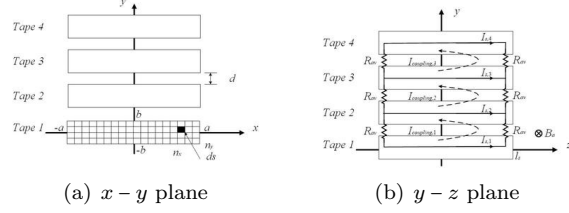


Figure 4: Sketch of modeling of partially coupled stack with resistance

The last integral can be neglected, since  $\mathbf{J}_s$  in the superconductor (and the  $\mathbf{A}_s$  that it generates) mostly follows the  $z$  direction, while  $\mathbf{J}_R$  (and its generated  $\mathbf{A}_R$ ) is mostly perpendicular to the  $z$  axis; and hence the dot product in the last integral above cancels.

Therefore, the total functional for very long tapes and neglecting dynamic effects in the resistances is

$$\begin{aligned}
 F \approx \int_{\Omega_{2D,s}} & \left[ \frac{1}{2} \frac{\Delta A_s}{\Delta t} \Delta J_s + \frac{\Delta A_a}{\Delta t} \Delta J_s + U(J_{s0} + \Delta J_s) \right] d^2 \mathbf{r} \\
 & + \sum_{j=1}^{n_R} \frac{1}{2} R_j I_j^2 - \sum_{i=1}^{n_t} V_i I_i - \sum_{j=1}^{n_R} V_j I_j.
 \end{aligned} \tag{18}$$

Since the resistive material is at the ends of the tapes, the current in each superconductor or resistance forms closed loops. Figure 4 shows our assumed circuits for the studied stacks, where only neighboring tapes are directly connected, but the following reasoning applies for any cross-connection between tapes. For any cross-connection, the last two terms in Table 18 can be grouped in closed loops, and hence they vanish due to the voltage Kirshoff law. For the example of figure 4, these two terms become

$$- \sum_{k=1}^{n_t} [V_{sk} - V_{s,k+1} + V_{Rk+} - V_{Rk-}] I_{\text{coupling},k}, \tag{19}$$

where  $I_{\text{coupling},k}$  is the coupling loop current of a particular loop  $k$ , and  $V_{Rk+}$ ,  $V_{Rk-}$  are the voltages at the right and left resistances of loop  $k$ , respectively. When writing the sum of voltages above as differences of potentials, it can be easily seen that it vanishes. Then, the functional to minimize is reduced to

$$\begin{aligned}
 F \approx \int_{\Omega_{2D,s}} & \left[ \frac{1}{2} \frac{\Delta A_s}{\Delta t} \Delta J_s + \frac{\Delta A_a}{\Delta t} \Delta J_s + U(J_{s0} + \Delta J_s) \right] d^2 \mathbf{r} \\
 & + \sum_{j=1}^{n_R} \frac{1}{2} R_j I_j^2.
 \end{aligned} \tag{20}$$

For our present case of figure 4, the last sum can be easily written in terms of

loop currents, with a resulting functional

$$\begin{aligned}
F \approx & \int_{\Omega_{2D,s}} \left[ \frac{1}{2} \frac{\Delta A_s}{\Delta t} \Delta J_s + \frac{\Delta A_a}{\Delta t} \Delta J_s + U(J_{s0} + \Delta J_s) \right] d^2 \mathbf{r} \\
& + \sum_{j=1}^{n_t-1} R_{av} I_{\text{coupling},j}^2.
\end{aligned} \tag{21}$$

The loop currents are related to the currents at each superconducting tape,  $I_i$  as

$$I_{\text{coupling},k} = \begin{cases} -I_1 & \text{for } k = 1 \\ I_{k-1} - I_k & \text{for } 1 < k < n_t - 1 . \\ I_{n_t} & \text{for } k = n_t - 1 \end{cases} \tag{22}$$

Therefore, the coupling loop currents are not independent variables. The reader should note that any coupling current distribution between tapes can be expressed as a linear combination of our defined loop coupling currents. For instance a loop flowing between the first and last tape corresponds to the case when the loop current in all unit loops is the same.

In order to find the solution of the current density by minimizing Table 21, we divide the tape cross-section into elements, being  $N$  the total number of elements in all tapes. To minimize Table 21, we can use an algorithm similar to that in [12]. Outlining, the algorithm follows the main steps below:

1. For each tape  $p$ , find the element pair within that tape,  $i_{p+}$  and  $i_{p-}$ , where applying a change in current  $+\delta I$  and  $-\delta I$  (with positive  $\delta I$ ), respectively, causes the smallest increment in  $F$ ,  $\delta F_j$ . For this, neglect the interaction between  $i_{p+}$  and  $i_{p-}$ , which can always be done for a high enough number of elements.
2. For each coupling loop,  $k$ , consisting of its upper and lower tape and its right and left resistances, find the element pair,  $i_{k+}$  and  $i_{k-}$ , with  $i_{k+}$  and  $i_{k-}$  belonging to different tapes where applying a change in current  $+\delta I$  and  $-\delta I$ , respectively, causes the smallest increment in  $F$ ,  $\delta F_k$ . Again, we neglect the interaction between  $i_{k+}$  and  $i_{k-}$  but now we need to take the resistance term in Table 21 into account. Naturally, for open circuit, where  $R_{av}$  is infinite,  $\delta F_k$  is also infinite, which will prevent setting currents in the coupling loops.
3. Choose the element pair, either within the same superconductor or in a coupling loop, where applying the change of current minimizes the functional the most.
4. If the change in the functional is negative, set this change of current in the related pair of elements. Then, calculate the new current in all tapes; and in all loops, if required. Any algorithm accelerators, such as the vector potential in the elements, should be calculated here, as done in [12]. Afterwards, repeat the process from step 1.

5. If the change of functional is non-negative, it means that we reached the unique minimum. Therefore, the routine ends.

For magnetic field dependent  $J_c$  (or other magnetic-field dependent parameters), we can solve the current density by combining this routine with the calculation of the magnetic field in an iterative way, as done in [12].

Once the current density is calculated, the power loss at time  $t$ ,  $P(t)$ , in the entire cross section is computed for each time step, being

$$\begin{aligned} P(t) &= P_s(t) + P_R(t) \\ &= l_s \sum_i^N J_i(t) E_i(t) s_i + 2 \sum_k^{n_{tape}-1} R_{av} I_{\text{coupling},k}^2(t), \end{aligned} \quad (23)$$

where the first and second terms are the superconductor and resistor loss, respectively. In this work, we distinguish between the superconductor and resistive loss, as occurring in the superconductor and in the resistive joints, respectively, instead of hysteresis and coupling loss [51]. The reason is that the coupling loss is difficult to define, since the coupling currents in the resistive joint create AC loss not only in the joint itself but also modify the AC loss in the superconductor, creating a frequency-dependent superconductor loss.

The loss  $Q$  over one cycle is obtained by the integration of Table 23.

$$\begin{aligned} Q &= Q_s + Q_R \\ &= \int_{mT}^{(m+1)T} P_s(t) dt + \int_{mT}^{(m+1)T} P_R(t) dt \end{aligned} \quad (24)$$

where  $T$  is the period and  $m$  is the number of periods having been computed, usually taken 0.5 (or more) for the stabilization of the calculated  $Q$ . Again, the first and second terms in Table 24 are the superconductor and resistor loss per cycle, respectively.

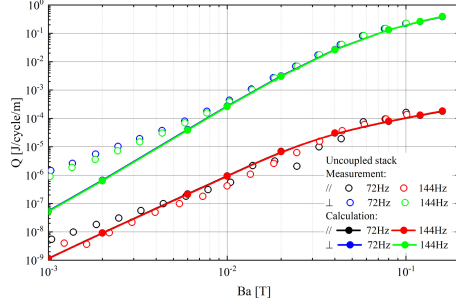
## 5 Results and discussion

The electromagnetic properties of the stack are solved by the minimum electromagnetic entropy production method programmed in C++.

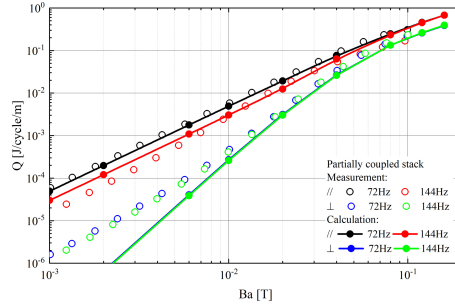
A stack with four tapes is modeled. The first superconducting tape of the stack is located at  $-a < x < a$ ,  $-b < y < b$  and meshed by  $n_x$  elements along x-axis and  $n_y$  elements along y-axis, respectively. Other tapes are located along y-axis with gap  $d = 1.5$  mm between tapes (see Figure 4(a)). Therefore, the total number of elements is  $N = n_{tape} \times n_x \times n_y$ , here  $n_{tape} = 4$ . We use the actual size of the superconducting layer with  $2a = 4$  mm width and  $2b = 2$   $\mu\text{m}$  thick is used to model superconductors. Proper mesh  $n_x = 5120$ ,  $n_y = 1$  and  $n_x = 40$ ,  $n_y = 64$  are chosen to calculate parallel and perpendicular applied sinusoidal magnetic field situation, respectively. We also use a tape length of 100 mm.

Furthermore, an analytical modeling of coupling loss for partially stack with four tapes for low frequency is deduced in A, which is valid for low frequencies. The average coupling power and coupling loss formulas are rewritten here,

$$\langle P \rangle = \frac{3\omega^2}{4R_{av}} (l_s \cdot d \cdot B_m)^2 \quad (25)$$



(a) Uncoupled stack



(b) Partially coupled stack

Figure 5: Magnetization loss of uncouple stack and partially coupled stack under parallel and perpendicular magnetic field, respectively. Loss  $Q$  is normalized to J/cycle/m. The amplitude of applied field increases from 1 mT to 100 mT at frequency 72 Hz and 144 Hz, respectively. The open circles are measurement results and the filled circles are calculation results. (a) Uncoupled stack. (b) Partially coupled stack.

$$\langle Q \rangle = \frac{3\pi\omega}{2R_{av}} (l_s \cdot d \cdot B_m)^2 \quad (26)$$

where  $R_{av}$  is the average resistance, and  $B_m$  is the amplitude of applied parallel magnetic field.

## 5.1 Amplitude dependence

The magnetization loss of uncoupled stack and partially coupled stack samples are measured and calculated for sinusoidal magnetic fields of amplitude ranging from 1 mT to 100 mT and frequency between 72 Hz and 144 Hz. The measurement and calculation results are presented in Figure 5.

Under parallel magnetic field situation, the induced current flows in  $y-z$  plane. For partially coupled stacks, the induced current flows across the soldered parts between tapes and causes coupling loss. The normalized magnetization

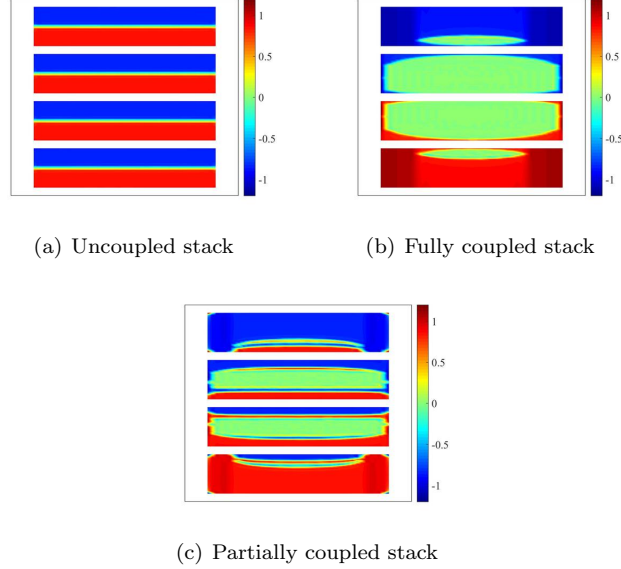


Figure 6: Current distribution of uncouple stack, fully coupled stack and partially coupled stack under parallel magnetic field, respectively when  $B_m = 0.02$  T,  $f = 72$  Hz,  $t/T = 1.25$ . The thickness of tape is scaled over 100 times to draw the distribution. (a) Uncoupled stack. (b) Fully coupled stack. (c) Partially coupled stack.

loss in partially coupled stacks increases from  $5 \times 10^{-5}$  to  $3 \times 10^{-1}$  J/cycle/m, which is over 3000 times higher than the loss in uncoupled stack. Since the uncoupled stack and partially coupled stack have the same configuration except the soldering parts, this great difference in magnetization loss mainly contributed by the coupling loss caused by the resistance between tapes.

Under perpendicular magnetic field situation, the current is induced within the superconducting tapes only, which flows in  $\pm z$  directions. Thus, partially the coupled stack has the same current distribution and the same loss as the uncoupled stack. When the amplitude increases from 1 mT to 100 mT, the normalized magnetization loss  $Q$  increases from  $1 \times 10^{-6}$  to  $2 \times 10^{-1}$  J/cycle/m. At low magnetic field amplitudes, measurements are higher than calculations. This could be caused by a possible degradation of the tape at edges [52]. With the increasing of magnetic field amplitude, the induced current penetrates from edges into the center, and hence edge damage effect is less important than before. Thanks to this, the calculations are almost the same as the measurements with a relative deviation smaller than 3%.

To show the great difference between the different kinds of stacks, Figures 6-9 present the current and electrical field distribution and profiles under applied magnetic field, respectively.

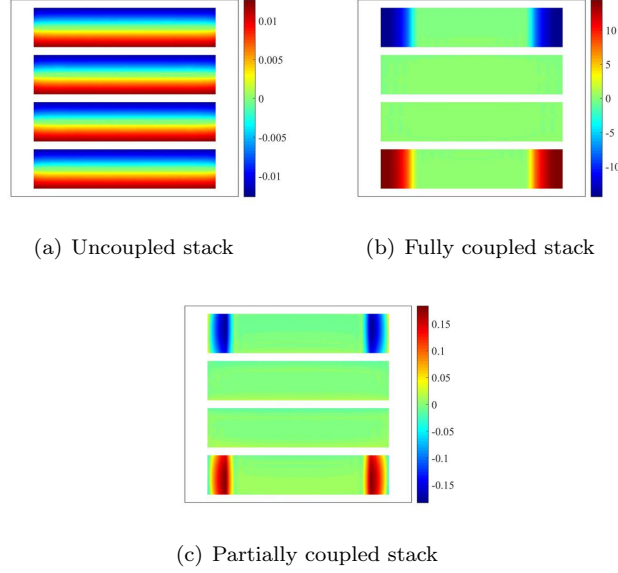


Figure 7: Electrical field distribution of uncouple stack, fully coupled stack and partially coupled stack under parallel magnetic field at  $B_m = 0.02$  T,  $f = 72$  Hz when  $t/T = 1.25$ , respectively. The thickness of tape is scaled over 100 times to draw the distribution. (a) Uncoupled stack. (c) Fully coupled stack. (e) Partially coupled stack.

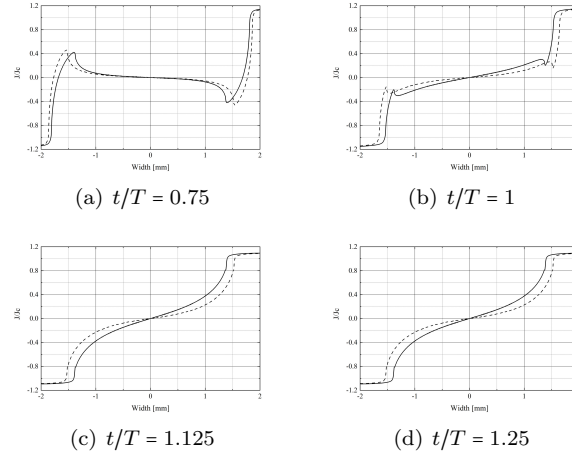


Figure 8: Current profiles of superconducting stack under perpendicular magnetic field at  $B_m = 0.02$  T,  $f = 72$  Hz when  $t/T = 0.75, 1, 1.125$  and  $1.25$ , respectively. The solid lines are the profiles of first tape and the dash lines are the profiles of second tape.

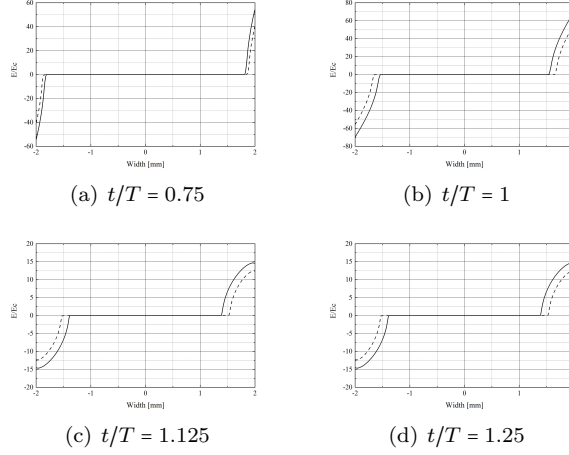


Figure 9: Electrical field profiles of superconducting stack under perpendicular magnetic field at  $B_m = 0.02$  T,  $f = 72$  Hz when  $t/T = 0.75, 1, 1.125$  and  $1.25$ , respectively. The solid lines are the profiles of first tape and the dash lines are the profiles of second tape.

Figure 6 shows the current distribution of these kinds of stack under parallel magnetic field at  $0.02$  T,  $72$  Hz when  $t/T = 1.5$ . For uncoupled stack, Figure 6(a), the induced current has fully penetrated into the center of each tape, because each tape is independent with no physical connection. For fully coupled stack, Figure 6(b), the induced current has penetrated in the first tape and a little bit in the second tape. There is no current in the center of stack, which performs like a superconducting bulk. Partially coupled stacks, Figure 6(c), perform similar to fully coupled stacks but there are some positive and negative currents in the center of the stack.

Figure 7 shows the electrical field distribution of these kinds of stack under parallel magnetic field. For the uncoupled stack, Figure 7(a), the electrical field distribution is almost the same in each tape. The peak positions appear at the thickness direction ( $y$  direction). For the fully coupled stack, Figure 7(b), the electrical field is almost zero everywhere except at the edges. For the partially coupled stack, Figure 7(c), the electrical field distribution is similar to the fully coupled stack but the peak positions appear at nearby edges and the amplitude of electrical field is much smaller than the fully coupled stack but larger than the uncoupled stack.

Figure 8 and Figure 9 are the current and electrical field profiles under perpendicular magnetic field when  $t/T = 0.75, 1, 1.125, 1.5$  at amplitude  $B_m = 0.02$  T and frequency  $f = 72$  Hz, respectively. The profiles of first (top) and the second (middle) tapes are drawn. When perpendicular magnetic field is applied on the stacks, the induced current flows only in the  $z$  direction and hence there is no coupling current between tapes. Therefore, the current and electrical field

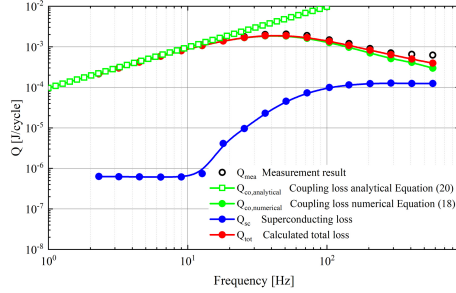


Figure 10: Magnetization loss of the partially coupled stack under parallel magnetic field at 18.7 mT with frequency ranging from 2 Hz to 576 Hz. The black circle line is measured total loss  $Q_{mea}$ , and the green open rectangle line is coupling loss  $Q_{co,analytical}$  calculated by analytical method Table 26. Others are numerical result calculated by Table 24: the green solid circle line is coupling loss  $Q_{co,numerical}$  (or resistor loss  $Q_R$  in the text), the blue solid circle line is superconducting loss  $Q_{sc}$  (or  $Q_s$  in the text). and the red solid circle line is calculated total loss  $Q_{tot}$ .

profiles of these three superconducting stacks are the same. With time changes from  $t/T = 0.75$  to 1.25, the amplitude of the magnetic field increases from the negative extreme value to the positive extreme value and the induced current and electrical field penetrates gradually from edges to center.

## 5.2 Frequency dependence

Figure 10 shows the superconducting loss and coupling loss of the partially coupled stack sample under parallel magnetic field. The coupling current at frequency 2.3 Hz, 36 Hz and 407 Hz are shown in Figure 11. The amplitude of parallel applied magnetic field is 18.7 mT and the frequency changes from 2 Hz to 576 Hz. When the frequency is below 10 Hz, the superconducting loss in the tapes  $Q_s$  is almost no frequency independent. When the frequency is above 10 Hz,  $Q_s$  increases sharply but it is still hundreds of times lower than the resistor loss  $Q_R$  in the soldering parts. However, when the frequency is higher than 100 Hz,  $Q_s$  increases much slower than before and trends to constant. Meanwhile,  $Q_R$  increases at the low frequency region and then decreases at the high frequency region. The maximum coupling loss appears at around 40 Hz, where the position of this maximum is related to the resistance and inductance.

The frequency dependence is mainly contributed by the resistances between tapes. The numerical result  $Q_{tot}$  is consistent with the measurement result  $Q_{mea}$  with a maximum relative error below 6%, which happens at high the frequency region. Furthermore, an analytical formulation of coupling loss for low frequency is deduced in Table 25, which agrees with numerical calculations and measurements at low frequency. However, when the frequency is higher than 300 Hz, the relative error is larger. The reason could be the eddy currents closing



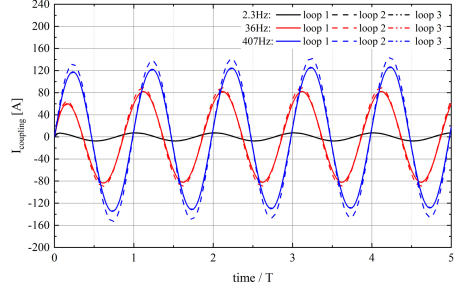


Figure 11: Coupling current of partially coupled stack under parallel magnetic field at 18.7 mT with frequency 2.3, 36, and 407 Hz. The solid line is the coupling current in loop 1, the dash line is the coupling current in loop 2, and the double dash line is the coupling current in loop 3. Because of the geometry symmetry of the stack, induced current in loop 1 and loop 3 are overlap each other.

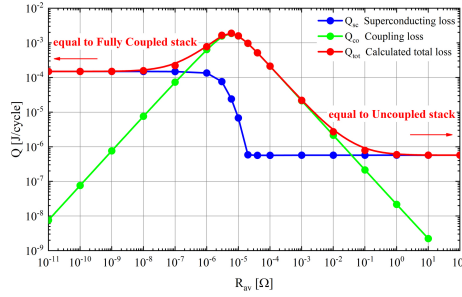


Figure 12: Magnetization loss of partially coupled stack under parallel magnetic field at 18.7 mT 72 Hz with average resistance ranging from  $1 \times 10^{-9} \Omega$  to  $1 \times 10^2 \Omega$ . The blue line is superconducting loss  $Q_{sc}$ , the green line is coupling loss  $Q_{co}$ , and the red line is the total loss  $Q_{tot}$ .

entirely within the soldering parts, which the model does not take into account. Another source of error could be inaccuracies in the superconducting loss calculation due to the constant  $J_c$ , which causes an increase in the superconducting loss.

### 5.3 Resistance dependence

Figure 12 shows the superconducting loss and coupling loss of the partially coupled stack sample under parallel magnetic field with amplitude 18.7 mT and frequency 72 Hz. The resistance changes from  $1 \times 10^{-10} \Omega$  to  $1 \times 10^2 \Omega$ . Figure 13 shows the coupling current of the partially coupled stack. Because of the geometrical symmetry of the stack, coupling currents in loop 1 and 3 are overlapped with each other. However, the coupling current in loop 2 is higher

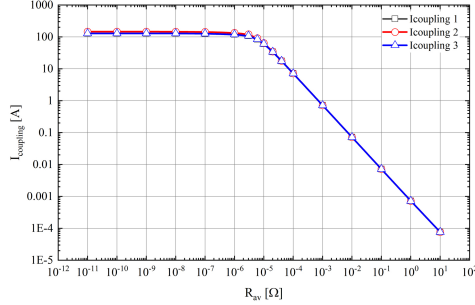


Figure 13: Coupling current (the amplitude per cycle) of partially coupled stack under 18.7 mT, 72 Hz parallel magnetic field with average resistance ranging from  $1 \times 10^{-9} \Omega$  to  $1 \times 10^2 \Omega$ . The black line is the coupling current in loop 1. The red line is the coupling current in loop 2. The blue line is the coupling current in loop 3.

than the others at the low resistance region.

With low resistances ( $R_{av} < 1 \times 10^{-6} \Omega$ ), the net current flowing between tapes is almost constant, which is entirely due to inductive effects. The value of the resistance is not playing any role, and hence the resistor loss  $Q_R$  decreases with the resistance  $R_{av}$ . The superconducting loss in the tapes  $Q_s$  is almost constant, which is about  $2 \times 10^{-4}$  J/cycle, while the resistor loss in the soldering parts  $Q_R$  is several orders of magnitude smaller than  $Q_s$ . Since the coupling current is fixed, see Figure 13, the Joule loss in the resistance  $R_{av} I_{coupling}^2$  increases linearly with the resistance. Intuitively, the case of  $R_{av} = 0 \Omega$  results in no resistor loss  $Q_{co} = 0$  J/cycle, since it corresponds to perfect shielding. Therefore, the total loss of the partially coupled stack  $Q_{tot}$  is almost the same as the fully coupled stack.

When the resistance is around  $7 \times 10^{-6} \Omega$ ,  $Q_R$  reaches the peak which is about  $2 \times 10^{-3}$  J/cycle. However, when the resistance is around  $1 \times 10^{-6} \Omega \sim 2 \times 10^{-5} \Omega$ , the coupling current decreases to zero sharply and  $Q_{sc}$  drops over 200 times. Since the coupling current is now dominated by the resistance, the coupling current decreases with  $R_{av}$ . This decrease is linear because the coupling current is so small that the applied magnetic field freely flows between tapes, causing an induced voltage independent on the coupling current and  $R_{av}$ . At last, coupling current cannot flow anywhere, and hence the total loss  $Q_{tot}$  is corresponds to that of the uncoupled stack.

#### 5.4 Length dependence

Figure 14 shows the magnetization loss of the partially coupled stack and Figure 15 is the coupling current with length increasing from 10 mm to 12800 mm. When the length is smaller than 100 mm, the superconducting loss in the tapes  $Q_s$  is about one thousand times smaller than  $Q_R$ . Since the resistance is con-

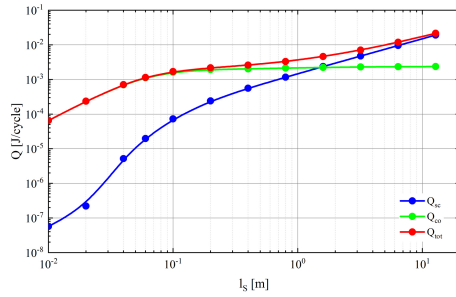


Figure 14: Magnetization loss of the partially coupled stack under 18.7 mT, 72 Hz parallel magnetic field with length ranging from 10 mm to 12800 mm. The black line is magnetization loss  $Q_{sc}$ , the red line is coupling loss  $Q_{cc}$ . And the blue line is total loss  $Q_{tot}$ . The loss unite is J/cycle.

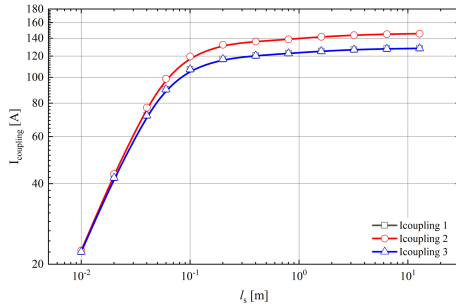


Figure 15: Coupling current in loops with length ranging from 10 mm to 12800 mm.

stant and the coupling current increases linearly with the length,  $Q_R$  increases following slope 2 in log-log scale. When the length is larger than 100 mm, the induced current in the superconducting tape trends to constant, and hence  $Q_R$  trends to constant but  $Q_s$  increases in proportion to the length. When the length further increases, the normalized total loss  $Q_{tot}$  is mainly contributed by  $Q_s$ .

## 6 Conclusion

A numerical 2D model is developed by the minimum electromagnetic entropy production (MEMEP) method to compute the coupling loss of partially coupled stacks. The presented MEMEP model shows the capability to take the resistance between tapes into account for coupling loss calculation with a high number of mesh elements. In addition, this model provides a remarkable good agreement with measurements.

This model is later used to systematically study the amplitude dependence, frequency dependence, resistance dependence, and length dependence of coupling loss. When a sinusoidal perpendicular magnetic field is applied on the stack samples, these superconducting stacks perform the same features and no obvious frequency dependence is observed. When a sinusoidal parallel magnetic field is applied, the total loss of partially coupled stack is much higher than the uncoupled stack. This is because there are resistances at the soldering parts that induce coupling loss. Obvious frequency dependence, resistance dependence and length dependence are detected in partially coupled stack too. With increasing frequency (or resistance), the coupling loss of the partially coupled stack increases at the beginning and then decreases. With the length of the sample increasing, the superconducting loss increases sharply at the beginning and then increases in proportion to the length, but the coupling loss in the soldered parts trends to constant.

At last, the 2D model presented here is useful for determining not just the value of predict the coupling loss but also other electromagnetic behavior in samples that are connected only at the ends, such as certain stacks of tapes, or coils with parallel tapes as conductor. This fast and accurate 2D model enables to study the effect of coupling at the current terminals of superconducting coils in complex systems, such as superconducting motors, where a full 3D model taking these effects into account is unfeasible due to its huge computing complexity.

## Acknowledgements

This paper is supported by European Commission Project Horizon 2020, No.723119 (ASuMED).

## References

## References

- [1] K. S. Haran, S. Kalsi, T. Arndt, H. Karmaker, R. Badcock, B. Buckley, T. Haugan, M. Izumi, D. Loder, J. W. Bray, P. Masson, and E. W. Stautner. High power density superconducting rotating machines-Development status and technology roadmap. *Supercond. Sci. Technol.*, 30(12):123002, 2017.
- [2] Advanced superconducting motor experimental demonstrator (ASuMED). <http://www.asumed.oswald.de/>.
- [3] Enric Pardo, Francesco Grilli, Yingzhen Liu, Simon Wolfädler, and Thomas Reis. Ac loss modeling in superconducting coils and motors with parallel tapes as conductor. *IEEE Transactions on Applied Superconductivity*, 29(5):1–5, 2019.
- [4] V. Grinenko, G. Fuchs, K. Nenkov, C. Stiehler, M. Vojenčiak, T. Reis, B. Oswald, and B. Holzapfel. Transport AC losses of YBCO pancake coils wound from parallel connected tapes. *Supercond. Sci. Technol.*, 25(7):075006, 2012.
- [5] E Pardo, M Kapolka, J Kováč, J Šouc, F Grilli, and A Piqué. Three-dimensional modeling and measurement of coupling AC loss in soldered tapes and striated coated conductors. *IEEE Trans. Appl. Supercond.*, 26(3):1–7, 2016.
- [6] Takeshi Mifune, Naoki Tominaga, Yusuke Sogabe, Yudai Mizobata, Masahiro Yasunaga, Akihiro Ida, Takeshi Iwashita, and Naoyuki Amemiya. Large-scale electromagnetic field analyses of coils wound with coated conductors using a current-vector-potential formulation with a thin-strip approximation. *Supercond. Sci. Technol.*, 32:094002, 2019.
- [7] R. Brambilla, F. Grilli, and L. Martini. Development of an edge-element model for AC loss computation of high-temperature superconductors. *Supercond. Sci. Technol.*, 20(1):16–24, 2007.
- [8] Huiming Zhang, Min Zhang, and Weijia Yuan. An efficient 3d finite element method model based on the t–a formulation for superconducting coated conductors. *Superconductor Science and Technology*, 30(2):024005, 2017.
- [9] Guole Liu, Guomin Zhang, Liwei Jing, Liwang Ai, Wanjie Li, Shizhuo Liu, and Qi Liu. Comparison of ac losses of ybco circular pancake coils and infinitely long stack approximation. *Journal of Superconductivity and Novel Magnetism*, 31(10):3141–3146, 2018.
- [10] Edgar Berrospe-Juarez, Víctor MR Zermeño, Frederic Trillaud, and Francesco Grilli. Real-time simulation of large-scale hts systems: multi-scale and homogeneous models using the t–a formulation. *Superconductor Science and Technology*, 32(6):065003, 2019.

- [11] Yawei Wang, Min Zhang, Francesco Grilli, Zixuan Zhu, and Weijia Yuan. Study of the magnetization loss of corc cables using 3d ta formulation. *Superconductor Science and Technology*, 2018.
- [12] Enric Pardo, Ján Šouc, and Lubomir Frolek. Electromagnetic modelling of superconductors with a smooth current–voltage relation: variational principle and coils from a few turns to large magnets. *Superconductor Science and Technology*, 28(4):044003, 2015.
- [13] E Pardo, M Kapolka, and J Souc. 3d and 2d electromagnetic modelling of superconductors: Flux cutting effects in finite samples and coated conductor coils up to 10 000 turns. In *Proc. 12th Eur. Conf. Appl. Supercond. (Lyon, France,)*, 2015.
- [14] M Kapolka, VMR Zermeno, S Zou, A Morandi, PL Ribani, E Pardo, and F Grilli. Three-dimensional modeling of the magnetization of superconducting rectangular-based bulks and tape stacks. *IEEE Transactions on Applied Superconductivity*, 28(4):1–6, 2018.
- [15] E Pardo and M Kapolka. 3D computation of non-linear eddy currents: variational method and superconducting cubic bulk. *Journal of Computational Physics*, 344:339–363, 2017.
- [16] E Pardo, F Gömöry, J Šouc, and JM Ceballos. Current distribution and ac loss for a superconducting rectangular strip with in-phase alternating current and applied field. *Superconductor Science and Technology*, 20(4):351, 2007.
- [17] Enric Pardo. Calculation of ac loss in coated conductor coils with a large number of turns. *Superconductor Science and Technology*, 26(10):105017, 2013.
- [18] M. Kapolka and E. Pardo. 3D modelling of macroscopic force-free effects in superconducting thin films and rectangular prisms. *Supercond. Sci. Technol.*, 32:054001, 2019.
- [19] E. Pardo, A. Sanchez, and C. Navau. Magnetic properties of arrays of superconducting strips in a perpendicular field. *Phys. Rev. B*, 67(10):104517, 2003.
- [20] F Grilli, SP Ashworth, and S Stavrev. Magnetization ac losses of stacks of YBCO coated conductors. *Physica C: Superconductivity*, 434(2):185–190, 2006.
- [21] Kazuhiro Kajikawa, K Funaki, K Shikimachi, N Hirano, and S Nagaya. Numerical evaluation of AC loss properties in assembled superconductor strips exposed to perpendicular magnetic field. *Physica C*, 469(15-20):1436–1438, 2009.

- [22] Z Hong and TA Coombs. Numerical modelling of AC loss in coated conductors by finite element software using H formulation. *Journal of Superconductivity and Novel Magnetism*, 23(8):1551–1562, 2010.
- [23] E. Pardo and F. Grilli. Numerical simulations of the angular dependence of magnetization AC losses: coated conductors, Roebel cables and double pancake coils. *Supercond. Sci. Technol.*, 25:014008, 2012.
- [24] N Bykovsky, G De Marzi, D Uglietti, P Bruzzone, and L Muzzi. Magnetization loss for stacks of rebco tapes. *Superconductor Science and Technology*, 30(2):024010, 2017.
- [25] Tatsuhito Ueno, Masataka Iwakuma, T Ito, Kiwook Yun, Kazuhisa Adachi, Akira Tomioka, Y Hase, Msayuki Konno, Teruo Izumi, Takato Machi, et al. AC loss properties of stacked REBCO superconducting tapes. *IEEE Transactions on Applied Superconductivity*, 27(4):1–6, 2017.
- [26] Vicente Climente-Alarcon, Anup Patel, Algirdas Baskys, and Bartek A Glowacki. Computation of superconducting stacks magnetization in an electrical machine. *IEEE Transactions on Applied Superconductivity*, 2019.
- [27] Mohammad Yazdani-Asrami, S Asghar Gholamian, Seyyed Mehdi Mirimani, and Jafar Adabi. Investigation on effect of magnetic field dependency coefficient of critical current density on the ac magnetizing loss in HTS tapes exposed to external field. *Journal of Superconductivity and Novel Magnetism*, 31(12):3899–3910, 2018.
- [28] E. Pardo. Modeling of coated conductor pancake coils with a large number of turns. *Supercond. Sci. Technol.*, 21:065014, 2008.
- [29] L. Prigozhin and V. Sokolovsky. Computing AC losses in stacks of high-temperature superconducting tapes. *Supercond. Sci. Technol.*, 24:075012, 2011.
- [30] Mark D Ainslie, Tim J Flack, and Archie M Campbell. Calculating transport AC losses in stacks of high temperature superconductor coated conductors with magnetic substrates using FEM. *Physica C: Superconductivity*, 472(1):50–56, 2012.
- [31] Victor MR Zermeno, Asger B Abrahamsen, Nenad Mijatovic, Bogi B Jensen, and Mads P Sørensen. Calculation of alternating current losses in stacks and coils made of second generation high temperature superconducting tapes for large scale applications. *Journal of Applied Physics*, 114(17):173901, 2013.
- [32] Wenjuan Song, Jin Fang, and Zhenan Jiang. Numerical ac loss analysis in hts stack carrying nonsinusoidal transport current. *IEEE Transactions on Applied Superconductivity*, 29(2):1–5, 2018.

- [33] F. Gömöry, M. Vojenčiak, E. Pardo, M. Solovyov, and J. Šouc. AC losses in coated conductors. *Supercond. Sci. Technol.*, 23:034012, 2010.
- [34] E. Pardo, J. Šouc, and M. Vojenčiak. AC loss measurement and simulation of a coated conductor pancake coil with ferromagnetic parts. *Supercond. Sci. Technol.*, 22:075007, 2009.
- [35] Guole Liu, Guomin Zhang, Liwei Jing, and Hui Yu. Numerical study on ac loss reduction of stacked hts tapes by optimal design of flux diverter. *Superconductor Science and Technology*, 30(12):125014, 2017.
- [36] Jun Ogawa, Satoshi Fukui, Tetsuo Oka, Tatsuya Sakurai, Yuki Sano, Hiroaki Tada, and Yuto Yoshii. Experimental investigation of ac loss characteristics of stacked hts tapes in an iron core. *IEEE Transactions on Applied Superconductivity*, 26(4):1–4, 2016.
- [37] V. Lahtinen, E. Pardo, J. Šouc, M. Solovyov, and A. Stenvall. Ripple field losses in DC biased superconductors: simulations and measurements. *J. Appl. Phys.*, 115:113907, 2013. arXiv:1308.6757.
- [38] Z Jiang, W Zhou, CW Bumby, M Staines, Q Li, RA Badcock, NJ Long, and J Fang. Dynamic resistance measurement of a four-tape ybco stack in a perpendicular magnetic field. *IEEE Transactions on Applied Superconductivity*, 28(4):1–5, 2017.
- [39] Mark D Ainslie, Chris W Bumby, Zhenan Jiang, Ryuki Toyomoto, and Naoyuki Amemiya. Numerical modelling of dynamic resistance in high-temperature superconducting coated-conductor wires. *Superconductor Science and Technology*, 31(7):074003, 2018.
- [40] Yanchao Liu, Zhenan Jiang, Quan Li, Chris W Bumby, Rodney A Badcock, and Jin Fang. Dynamic resistance measurement in a four-tape YBCO stack with various applied field orientation. *IEEE Transactions on Applied Superconductivity*, 29(5):1–7, 2019.
- [41] Mark Douglas Ainslie and H Fujishiro. Modelling of bulk superconductor magnetization. *Superconductor Science and Technology*, 28(5):053002, 2015.
- [42] S Zou, VMR Zermeño, A Baskys, A Patel, F Grilli, and BA Glowacki. Simulation and experiments of stacks of high temperature superconducting coated conductors magnetized by pulsed field magnetization with multi-pulse technique. *Supercond. Sci. Technol.*, 30(1):014010, 2017.
- [43] A. Campbell, M. Baghdadi, A. Patel, D. Zhou, K. Y. Huang, Y. Shi, and T. Coombs. Demagnetisation by crossed fields in superconductors. *Supercond. Sci. Technol.*, 30(3):034005, 2017.



- [44] F. Liang, T. Qu, Z. Zhang, J. Sheng, W. Yuan., Y. Iwasa, and M. Zhang. Vortex shaking study of REBCO tape with consideration of anisotropic characteristics. *Supercond. Sci. Technol.*, 30(9):094006, 2017.
- [45] M. Baghdadi, H. S. Ruiz, and T. A. Coombs. Nature of the low magnetization decay on stacks of second generation superconducting tapes under crossed and rotating magnetic field experiments. 8:1342, 2018.
- [46] Xiang Li, Jing Li, Pengbo Zhou, Kun Liu, Le Han, Xuliang Song, and Guangtong Ma. Decay of trapped magnetic field in stacks of YBCO coated conductors subjected to traveling magnetic waves. *IEEE Transactions on Applied Superconductivity*, 29(7):1–9, 2019.
- [47] M. Kapolka, J. Srpčić, D. Zhou, M. D. Ainslie, E. Pardo, and A. R. Dennis. Demagnetization of cubic Gd-Ba-Cu-O bulk superconductor by crossed-fields: Measurements and three-dimensional modeling. *IEEE Trans. Appl. Supercond.*, 28(4):1–5, 2018.
- [48] M Kapolka, E Pardo, F Grilli, A Baskys, V Climente-Alarcon, and B A Glowacki. Cross-field demagnetization of stacks of tapes: 3D modelling and measurements. *arXiv preprint arXiv:1909.12129*, 2019.
- [49] Naoyuki Amemiya, Satoshi Kasai, Keiji Yoda, Zhenan Jiang, George A Levin, Paul N Barnes, and Charles E Oberly. Ac loss reduction of YBCO coated conductors by multifilamentary structure. *Superconductor Science and Technology*, 17(12):1464, 2004.
- [50] Ján Šouc, Fedor Gömöry, and Michal Vojenčiak. Calibration free method for measurement of the ac magnetization loss. *Superconductor Science and Technology*, 18(5):592, 2005.
- [51] F. Grilli, E. Pardo, A. Stenvall, D. N. Nguyen, W. Yuan, and F. Gömöry. Computation of losses in HTS under the action of varying magnetic fields and currents. *IEEE Trans. Appl. Supercond.*, 24(1):8200433, 2014.
- [52] Mykola Solovyov, Enric Pardo, Ján Šouc, Fedor Gömöry, Michal Skarba, Pavol Konopka, Marcela Pekarčíková, and Jozef Janovec. Non-uniformity of coated conductor tapes. *Superconductor Science and Technology*, 26(11):115013, 2013.

## A Coupling loss analytical modeling for low frequency

In this section, coupling loss of partially coupled stack at low frequency is deduced. There are four tapes in stack.

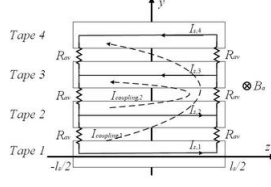


Figure 16: Sketch of partially coupled stack for analytical modeling. (cross section in y-z platform )

When a parallel magnetic field is applied on the partially coupled stack, the coupling current is induced which obey Ampere' Law.

$$\oint d\vec{S} \cdot \vec{B}_a = L\dot{I} + \dot{B}_a \cdot d \cdot l_s \quad (27)$$

where  $d$  is the gap between tapes.  $l_s$  is the length of tape.  $L$  is the inductance of the superconductor loop which is neglect-able at low frequency. Based on Faraday' Law,

$$R_{av}I = -\frac{1}{2} \cdot d \cdot l_s \cdot \dot{B}_a - \vec{E}_s \cdot l_s \quad (28)$$

Because  $I \ll I_c$ , the electromotive  $E_s$  on superconducting tapes approximate zero. So,

$$R_{av}I = -\frac{1}{2} \cdot d \cdot l_s \cdot \dot{B}_a \quad (29)$$

where  $B_a$  is parallel applied magnetic field,  $B_a = B_m \sin \omega t$ . And  $\dot{B}_a = \partial B_a / \partial t = \omega B_m \cos \omega t$ ,  $B_m$  is the amplitude of the applied parallel magnetic field.

As shown in Figure 16, because of the geometry symmetry of the partially coupled stack, tape No. 1 and No. 4 form a big current loop and tape No. 2 and No. 3 form another current loop. So, induced currents in tapes are written as

$$I_{s,1} = -\frac{l_s}{2R_1} (\dot{B}_a \cdot d_1) \quad (30)$$

$$I_{s,2} = -\frac{l_s}{2R_2} (\dot{B}_a \cdot d_2) \quad (31)$$

And induced current in tape No.3 and No. 4 are written as  $I_{s,4} = -I_{s,1}$  and  $I_{s,3} = -I_{s,2}$ , respectively.

Because  $R_1 = 3R_{av}$ ,  $R_2 = R_{av}$ ,  $d_1 = 3d$ , and  $d_2 = d$ , power loss in resistance is deduced,

$$\begin{aligned} P(t) &= 2(R_1 - R_2)I_{s,1}^2 + 2R_2(I_{s,1} + I_{s,2})^2 \\ &= \frac{3}{2R_{av}} (l_s \cdot d \cdot \omega B_m \cos \omega t)^2 \end{aligned} \quad (32)$$

And average power loss is

$$\langle P \rangle = \frac{3\omega^2}{4R_{av}} (l_s \cdot d \cdot B_m)^2 \quad (33)$$

$$\langle Q \rangle = \langle P \rangle / f = \frac{3\pi\omega}{2R_{av}} (l_s \cdot d \cdot B_m)^2 \quad (34)$$

## B Coupling loss analytical modeling for any frequency

In this section, coupling loss of partially coupled stack at high frequency is deduced by analytical method. To simplify the issue, only two superconducting tapes in closed loop are considered.

At high frequency, the inductance is not negligible anymore.

$$L = d \cdot l_s \cdot \mu_0 / W \quad (35)$$

where,  $W$  is the width of tape.  $d$  is the gap between tapes.  $l_s$  is the length of tape.

Table 29 is revised to

$$R_{av}I + \frac{1}{2}L\dot{I} = -\frac{1}{2} \cdot d \cdot l_s \cdot \dot{B}_a \quad (36)$$

where,  $R_{av}$  is the average resistance in closed loop. And for any current can be written in Fourier decomposition form,

$$\begin{aligned} I &= I_{co} \cos \omega t + I_{si} \sin \omega t \\ \dot{I} &= -\omega I_{co} \sin \omega t + \omega I_{si} \cos \omega t \end{aligned} \quad (37)$$

where  $I_{co}$  and  $I_{si}$  are two components of the induced current.

Take Table 37 into Table 36 to solve the  $I_{si}$  and  $I_{co}$ .

$$\begin{cases} I_{si} - \frac{\omega L}{2R_{av}} \cdot I_{co} = 0 \\ I_{co} + \frac{\omega L}{2R_{av}} \cdot I_{si} + \frac{1}{2R_{av}} \cdot d \cdot l_s \cdot \omega B_m = 0 \end{cases} \quad (38)$$

So, we can deduce

$$I_{co} = -\frac{1}{2R_{av}} \cdot d \cdot l_s \cdot \omega B_m \cdot \frac{1}{1 + \left(\frac{L\omega}{2R_{av}}\right)^2} \quad (39)$$

$$I_{si} = -\frac{1}{2R_{av}} \cdot \frac{\omega L}{2R_{av}} \cdot d \cdot l_s \cdot \omega B_m \cdot \frac{1}{1 + \left(\frac{L\omega}{2R_{av}}\right)^2} \quad (40)$$

Then, the coupling power is

$$\begin{aligned} P(t) &= 2R_{av}I^2 \\ &= 2R_{av} \cdot (I_{co} \cos \omega t + I_{si} \sin \omega t)^2 \\ &= \frac{(\cos \omega t + \frac{L\omega}{2R_{av}} \cdot \sin \omega t)^2}{2R_{av}} \cdot \left( \frac{d l_s \cdot \omega \cdot B_m}{1 + \left(\frac{L\omega}{2R_{av}}\right)^2} \right)^2 \end{aligned} \quad (41)$$

So, average coupling loss is

$$\langle P \rangle = \frac{1}{4R_{av}} \cdot (d \cdot l_s \cdot \omega \cdot B_m)^2 \cdot \frac{1}{1 + (\frac{L\omega}{2R_{av}})^2} \quad (42)$$

$$\begin{aligned} \langle Q \rangle &= \langle P \rangle / f \\ &= \frac{\pi\omega}{2R_{av}} \cdot (d \cdot l_s \cdot B_m)^2 \cdot \frac{1}{1 + (\frac{L\omega}{2R_{av}})^2} \end{aligned} \quad (43)$$

■ **Amplitude dependency**

Because,

$$\frac{d \langle Q \rangle}{dB_m} = \frac{\pi\omega \cdot (d \cdot l_s)^2}{R_{av}} \cdot \frac{B_m}{1 + (\frac{L\omega}{2R_{av}})^2} > 0 \quad (44)$$

The coupling loss is always increasing linearly with amplitude at a specific rate which is related to  $\omega$  and  $R_{av}$ .

■ **Frequency dependency**

When  $\omega = 2R_{av}/L$ ,  $d \langle Q \rangle / d\omega = 0$ .

$$\begin{aligned} \frac{d \langle Q \rangle}{d\omega} &= \frac{\pi \cdot (d \cdot l_s \cdot B_m)^2}{2R_{av}} \cdot \frac{1 - (\frac{L\omega}{2R_{av}})^2}{[1 + (\frac{L\omega}{2R_{av}})^2]^2} \\ &= 0 \end{aligned} \quad (45)$$

The peak value of coupling loss is

$$\langle Q_{co} \rangle_f = \frac{\pi}{2L} \cdot (d \cdot l_s \cdot B_m)^2 \quad (46)$$

The peak value of  $\langle Q_{co} \rangle_f$  is only related to the geometry of the stack and the amplitude of applied magnetic field but is not related to  $R_{av}$ . So, once the geometry is fixed, the peak value of frequency dependency is constant.

■ **Resistance dependency**

When  $R_{av} = L\omega/2$ ,  $d \langle Q \rangle / dR_{av} = 0$ .

$$\begin{aligned} \frac{d \langle Q \rangle}{dR_{av}} &= \frac{\pi\omega \cdot (d \cdot l_s \cdot B_m)^2}{2} \cdot \frac{(\frac{L\omega}{2})^2 - R_{av}^2}{[R_{av}^2 + (\frac{L\omega}{2})^2]^2} \\ &= 0 \end{aligned} \quad (47)$$

So, the peak value of coupling loss is

$$\langle Q_{co} \rangle_R = \frac{\pi}{L} \cdot (d \cdot l_s \cdot B_m)^2 \quad (48)$$

The peak value of  $\langle Q_{co} \rangle_R$  is only related to the geometry of the stack and the amplitude of applied magnetic field but is not related to  $\omega$ .

■ **Gap ( $d$ ) dependency or length ( $l_s$ ) dependency**

$$\frac{d \langle Q \rangle}{dd} = \frac{\pi\omega \cdot (l_s \cdot B_m)^2}{2R_{av}} \cdot \frac{2d}{[1 + (\frac{L\omega}{2R_{av}})^2]^2} \geq 0 \quad (49)$$

$$\frac{d \langle Q \rangle}{dl_s} = \frac{\pi\omega \cdot (d \cdot B_m)^2}{2R_{av}} \cdot \frac{2l_s}{[1 + (\frac{L\omega}{2R_{av}})^2]^2} \geq 0 \quad (50)$$

so,  $\langle Q \rangle$  is always monotone increasing with gap and length.